Original Article

Institution of MECHANICAL ENGINEERS
Journal of MECHANICAL ENGINEERING SCIENCE

Proc IMechE Part C:
J Mechanical Engineering Science
2017, Vol. 231(11) 1995–2004

DOI: 10.1177/0954406215626941
journals.sagepub.com/home/pic
SAGE

# Mechanical characterization and finite element modeling of polylactic acid BCC-Z cellular lattice structures fabricated by fused deposition modeling

**R Rezaei, MR Karamooz Ravari, M Badrossamay and M Kadkhodaei**

**Abstract**

In recent years, cellular lattice structures are of interest due to their high strength in combination with low weight. They may be used in various areas such as aerospace and automotive industries. Accordingly, assessment of their manufacturability, repeatability and mechanical properties is very important. In this paper, these issues are investigated for Polylactic Acid cellular lattice structures fabricated by fused deposition modeling. To do so, some benchmarks are designed and fabricated to find suitable processing parameters as well as the structural dimensions. In addition, to evaluate the mechanical properties of the lattice's material, a number of tension and compression specimens are fabricated and tested. The material's stress–strain curves reveal non-linear behaviors. These curves are not coincided in tension and compression which shows an asymmetric material behavior. To characterize the fabricated cellular lattices, they are tested in compression, and the deformation mechanisms of the structures are analyzed. To investigate the correlation between the bulk material and the material of the ligaments, a solid finite element model is developed to predict the stress–strain response of the lattice. The obtained result shows a reasonably good correlation between the model and experiments.

**Keywords**

Cellular lattice structure, fused deposition modeling, polylactic acid, additive manufacturing, mechanical characterization, finite element

Date received: 17 December 2015; accepted: 22 December 2015

## Introduction

Additive manufacturing processes (AM) allow gaining innovative parts with complex geometry directly from three-dimensional computer aided design (CAD) models.[1–3] In addition, some of these techniques are capable of fabricating not only prototypes but also end-use parts with good mechanical properties as well as geometric agreements with original CAD models.[2–4] Moreover, these techniques make the ability of fabricating lightweight, strong parts with internal pores to save expensive functional materials in a reasonable time.[2,3,5]

Since lightweight parts have significant benefits, cellular lattice structures (CLS) have been receiving considerable attention in the past few decades.[6] These constructions have an internal porous structure that may be either stochastic (e.g. closed or open foams) or periodic. Periodic architectures are considered by a unit cell that can be repeated in two or three directions to create a desired part.[6,7] Nowadays, CLSs are widely used in various engineering and medical applications including energy absorbers, packaging devices, automotive parts, scaffolds in tissue engineering, heat exchangers, and sound and thermal insulators.[3,6–9]

Regarding metallic lattice truss structures, several approaches have been used to fabricate and to characterize them. For instance, they can be made by perforating a metal sheet with a periodic pattern followed by folding at node rows to create a plate of 3D interconnected trusses.[9] Kooistra[10] fabricated lattice structures by using perforated aluminum sheets and carried out a number of experimental compression tests on

Department of Mechanical Engineering, Isfahan University of Technology, Isfahan, Iran

**Corresponding author:**
MR Karamooz Ravari, Department of Mechanical Engineering, Isfahan University of Technology, 84156-83111 Isfahan, Islamic Republic of Iran.
Email: m.karamoozravari@me.iut.ac.ir

the products. Since the initial sheet that was used to make lattice structure was inefficiently utilized, a new method was introduced by Kooistra and Wadley[9] to efficiently use the sheets. Several researchers have used the AM processes to fabricate the cellular lattice structures. Among the proposed methods, selective laser melting (SLM), as a powder-bed fusion (PBF) process for the direct fabrication of functional metallic parts,[11] is of more importance. Bael et al.[12] fabricated a number of Ti6Al4V scaffolds through SLM. They also performed mechanical and geometrical tests to examine repeatability of the process. Hollow truss structures were investigated by Wadley and Queheillalt[7] not only to use their high mechanical strength but also to increase efficiency in heat transfer capability of these structures. Tsopanos et al.[13] fabricated BCC microstructure lattice using SLM to assess the influence of processing parameters on their mechanical properties. They also reported the stress–strain curve of the micro struts and calibrated these curves using finite element simulations. Labeas and Sunaric[14] fabricated three different cellular core types and developed a methodology to predict mechanical properties and deformation behavior of the structure using finite element method. Their obtained results were compared with the experimental measurements.[13] Yan et al.[3] investigated the possibility of manufacturing lattice structures with different unit cell sizes using SLM process. They also assessed the mechanical properties of each part. Correlation between yield strength and relative density of parts fabricated by selective laser sintering (SLS) process was assessed by Ceradi et al.[2] Through static compression tests, Gumruk and Mines[6] investigated the mechanical behavior of stainless steel lattice structures fabricated by SLM process.

Manufacturability is a very important issue when designing a CLS. For instance, in some cases, the part cannot be built with a specific process or the quality of fabricated part would not be acceptable. In addition, lattice structures have a very complex internal structure so that supportive structures might be used to prevent part's overhanging and deformation. These supports are often not acceptable because not only they would be difficult to be removed from the main structure, but also they cause waste of the material and time.[3] Accordingly, it is very important to investigate limitations of the process before designing and fabricating parts.[15]

The main aim of the present study is to investigate the manufacturability and repeatability of Polylactic Acid BCC-Z CLS fabricated by fused deposition modeling (FDM) using a laboratory inexpensive FDM machine. To this end, a systematic approach is implemented in which a number of benchmarks are designed to obtain the minimum value of struts' diameter, appropriate diagonal struts' angles, and fabrication speed. According to these benchmarks, three BCC-Z CLSs with the porosity of about 92% are fabricated and examined under mechanical compression. The obtained mechanical properties of the structures reveal a good repeatability. In addition, the compressive load-carrying capacity of the fabricated CLS's is found to be about 150 kg at its ultimate point while its weight is about 5.2 g. In addition, to evaluate the mechanical properties of the lattice's struts material, a number of tension and compression specimens are fabricated and tested. The stress–strain curves of the bulk material in tension and compression illustrate asymmetric material properties. To evaluate relationships between the bulk samples with the CLSs' struts, a solid finite element model is developed, and the stress–strain response of the bulk material in compression is attributed to the struts' material. The stress–strain response in elastic region shows a very good agreement with the experimentally obtained one.

The rest of the paper is organized as follows: the following section describes the material and methods containing fabrication of the cellular lattices, mechanical characterization of the specimens, and the solid finite modeling of the structure. In the Results and discussion section, the results of both experimental measurements and finite element model are presented and discussed. Finally, the paper ends with conclusions of the present study in the Conclusion section.

## Materials and methods

This section starts with the procedure of the design and fabrication of the studied CLSs in this study. In the second part, the mechanical characterization of cellular lattice structures as well as tension and compression specimens is explained in detail. The last subsection is allotted to the finite element modeling approach for predicting the mechanical stress–strain response of the lattices.

### *Specimen design and fabrication*

One of the main goals of the present study is to evaluate the manufacturability of FDM process for fabrication of Polylactic Acid CLS's. It has been previously shown[16,17] that 'angle-ply' lattices, whose struts are oriented in 45°, offer nearly optimized configurations under bending, compression, and shear loadings. Accordingly, in this work, a BCC-Z topology is used to develop the lattice structure. As shown in Figure 1(a), the BCC-Z unit cell can be described as a structure with 10 struts, eight of which connects the center of a cube to its corners and the other two connect the center of the cube to the center of its upper as well as lower face. The structure is generated through commercial FEM software using a set of vertices and connections among them. Figure 1(b) shows a 2D view of the wire frame of the lattice structure. Notice that, in this model, no diameter has been assigned to the

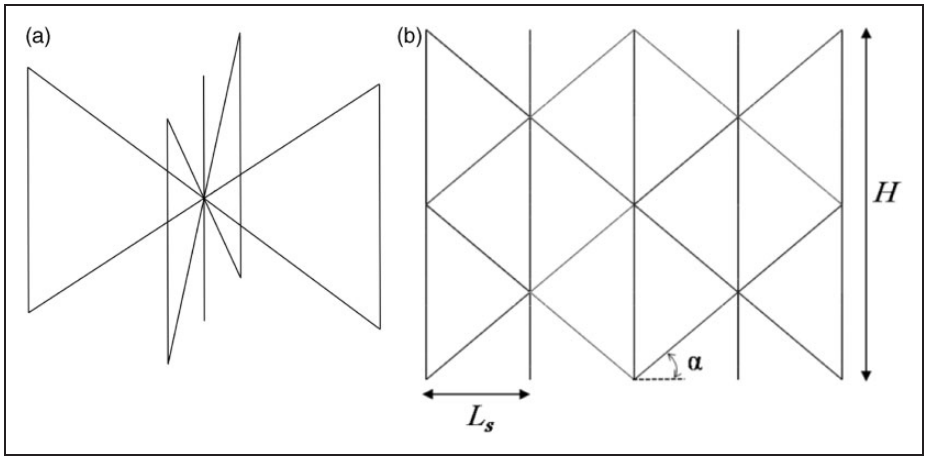


**Figure 1.** The cellular lattice structure designed in the commercial FEM software: (a) 3D view and (b) side view.

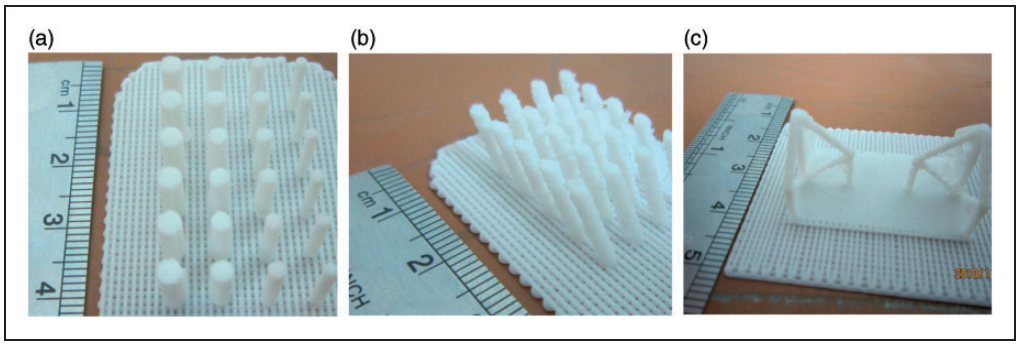


**Figure 2.** Three designed benchmarks to obtain (a) the minimum diameter, (b) the minimum angle of struts, and (c) the processing parameters.

struts. The appropriate diameter will be found in the following steps.

The CLS can be fully defined using four parameters: the vertical struts distance ($L_s$), the angle of diagonal struts ($\alpha$), the whole structure height (H), and diameter of the struts. All of these parameters, except the diameter of the struts, are shown in Figure 1(b). Among these parameters, strut distances, diameter of the struts, and angle of diagonal struts may affect the manufacturability of the process.

The modeled part is saved in STL format, and the open-access slicing software AXON 2 is then used to import the designed part to the fused deposition modeling (FDM) system. This system is a laboratory extrusion-based AM apparatus, RAPMAN 3.2, containing a polylactic acid polymer[a] filament with the diameter of 3 mm as raw material for fabricating the parts. It has been previously shown that decrease in the layer thickness in FDM process decreases the surface roughness[18] while it increases the compressive strength[19] and the processing time.[20] Since minimum surface roughness and higher load-bearing capacity are of interest, the minimum available value of layer thickness is chosen in the present work. Accordingly, the processing parameters used in this study are as follows: the layer thickness is 0.125 mm; the maximum extrusion temperature for material is195 °C; and the laboratory temperature is about 25 °C. Considering these parameters, three benchmarks are designed and fabricated. Accordingly, proper geometric and fabrication parameters are obtained. Prior to conducting the foregoing experiments, two geometric benchmarks are proposed, designed and fabricated to evaluate the performance of the FDM machine/process. The first benchmark is designed to obtain suitable diameter of vertical struts as shown in Figure 2(a). It contains six columns of struts whose diameter in each column is 1.5, 2, 2.5, and 3 mm. It is worth mentioning that a row of struts with the diameter of 1 mm is also considered. However, it is not possible to fabricate it due to the limitations of the machine. Therefore, the diameter is increased to those reported above. The second type of benchmark is designed to find the achievable strut diameter and the corresponding angle for diagonal struts. As shown in Figure 2(b), four columns of struts with the angles of 35, 40, 45, and 50° are fabricated for each strut diameter obtained using the first benchmark findings. Therefore, the proper angle and diameter are resulted using these two benchmarks. It is

[a]Polylactic Acid is a thermoplastic aliphatic polyester derived from renewable resources such as corn starch, tapioca roots, chips or starch, or sugarcane.

realized that the minimum struts' angle with an acceptable quality is about 40°. Accordingly, this value is utilized for the design of the lattice.

Due to inherent geometrical complexity in CLS, the manufacturing process is associated with severe vibrations caused by fast movement of the extruding nozzle. Since the vertical and diagonal struts are near each other in the CLS, this vibration may give rise to some difficulties. Considering this issue, another type of benchmark is designed to figure out the proper methodology, which has to be applied to obtain the desired CLS. This benchmark is comprised of two unit cells as illustrated in Figure 2(c). In this benchmark, the diameter of the struts is 1.5 mm and the angle of 40° is selected for the diagonal struts. In order to enhance the rigidity of the benchmark and to deal with poor attachment between struts and the base plate, a thin plate is designed under these benchmarks as well as the CLS. Although fabrication of struts with bigger angles is easier, fabrication time decreases by decrease in the total height of the structure. Consequently, it is preferable to design the diagonal struts with the minimum achievable angle. Notice that the angle of diagonal struts is in a direct relationship to the whole structure's height.

The dimensions of CLS are finalized based on the results achieved through investigation of the benchmarks. Figure 3 shows the final version of the structure with its dimensions. According to the obtained dimensions, the porosity of the CLS is calculated to be about 90.22% using the CAD model.

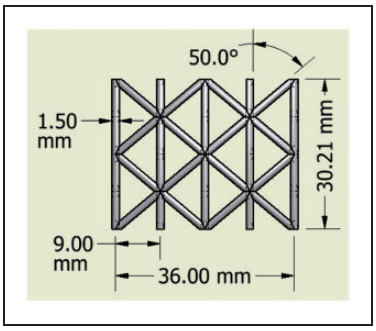


**Figure 3.** Side view of the final version of the cellular lattice structure.

## Mechanical behavior characterization

Since mechanical behavior is one of the most important characteristics that are expected from cellular lattice structures, some relevant experimental measurements are carried out. As the mechanical properties of the bulk material of a part can be affected by the fabrication method, it is worthwhile to assess the mechanical properties of the bulk material as well. To achieve this goal, a number of tension and compression specimens are fabricated using the same processing parameters as those applied to fabricate CLSs. The tension and compression specimens are designed according to ASTM D638[21] and ASTM D695,[22] respectively, which are suitable for rigid and semi-rigid plastics. Tension and compression tests are carried out using SANTAM, STM-50 tensile apparatus depicted in Figure 4.

In the next stage, the static behavior of the CLS is investigated using the compression test. The first cellular lattice structure is examined with the strain rate of about $10^{-4}\,S^{-1}$. As shown in Figure 5(a), the deformation is localized near the moving platen illustrating that there is a dynamic loading on the structure. As a consequence, the velocity of the upper platen should be decreased. For other specimens, the strain rate is reduced to $10^{-5}\,S^{-1}$. Figure 5(b) shows deformation of the structure during the test using the strain rate of about $10^{-5}\,S^{-1}$. As is seen, a uniform deformation occurs in the struts of the structure.

## Finite element modeling

In this section, finite element method is used to simulate the stress–strain response of the cellular lattice structure fabricated by FDM. To do so, a PYTHON script is developed through ABAQUS 6.11-1 to construct the finite element model of the lattice as shown in Figure 6. The diameter of the fabricated lattices' struts is measured in several points,

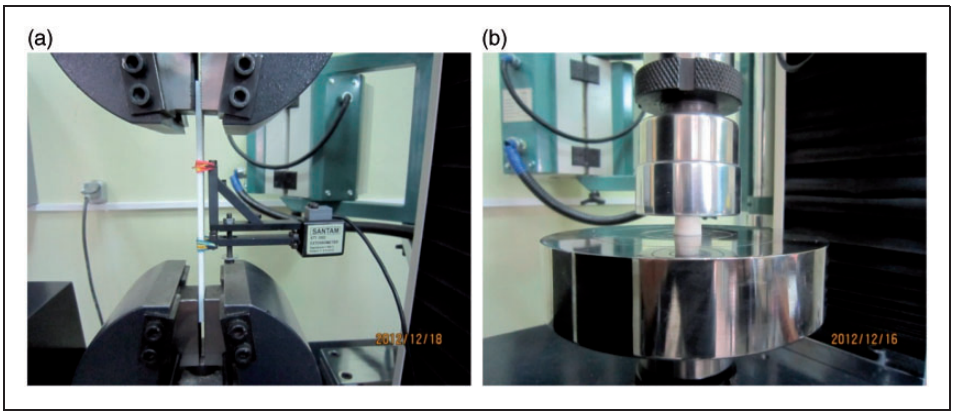


**Figure 4.** Illustration of (a) tension and (b) compression tests.

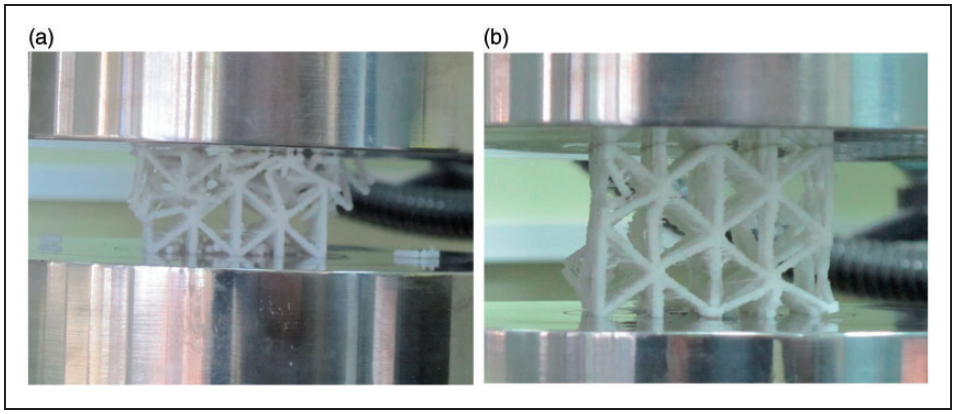


**Figure 5.** (a) Deformation localization in the struts with the use of the strain rate of about $10^{-4}\,S^{-1}$, and (b) uniform deformation by using the strain rate of about $10^{-5}\,S^{-1}$.

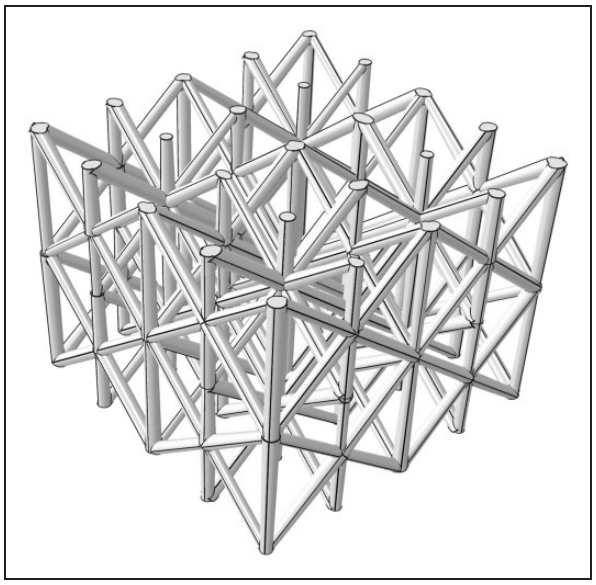

**Figure 6.** The finite element model of the lattice.

and the average value is calculated to be about 1.482 mm. It is supposed that the diameter of the struts is constant along their length, and the calculated average value is assigned as the diameter of all the struts.

The boundary conditions shown in Figure 7 are applied to the model in order to resemble the experiments. Since the friction between the loading platens and the lattice is not negligible, all the translational degrees of freedom perpendicular to the loading direction are constrained. In the loading direction, the translational degree of freedom of the nodes on the bottom plane of the model is fixed while those of the upper plane are forced to move downward to compress the lattice. The stress and strain are calculated using equations (1) and (2), respectively.

$$\sigma = \frac{\sum F_i}{A} \tag{1}$$

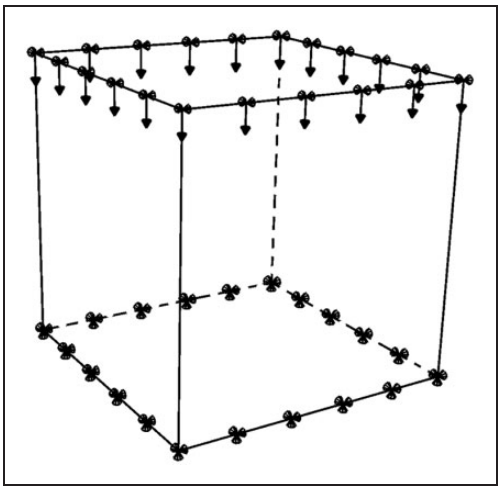

**Figure 7.** Schematic of the boundary conditions applied to the model.

$$\varepsilon = \frac{\delta}{H} \tag{2}$$

in which $F_i$ is the reaction force of the i-th node in the upper plane, A the projection of the lattice's area on the plane parallel to the loading plane, δ the displacement of the upper plane nodes, and H the height of the lattice.

Referring to Figure 8, the model is meshed using second-order accuracy tetrahedral continuum elements, denoted as C3D10M in ABAQUS, to be able to capture the complex geometry of the struts (especially in conjunction of the struts) and to avoid numerical problems.[23]

## Results and discussion

### *Bulk material characterization*

To simulate the mechanical response of CLSs, it is necessary to know about both internal structure and the mechanical properties of the bulk material of the CLS in tension and compression. Therefore, in this

section, the mechanical properties of the bulk material of the CLS are presented.

As mentioned in the previous section, a number of specimens are prepared for each of the bulk tension, bulk compression, and that CLS compression tests. Then, for each of these specimens, the average stress-strain curve is reported. Both bulk tension and compression tests are carried out at the strain rate of $2 \times 10^{-4}\,S^{-1}$. Figure 9 shows the stress–strain curve of tension specimens. It is observed that there is a large variation in the slope of the curve in a certain strain. This variation can be found in all tested specimens but not at the same corresponding strains. In the first region of the curve, called the toe region, the PLA fibers begin to align in the direction of the stress that is called un-crimping. Resultantly, a small stress can cause a large strain in the first region. In the next region, the fibers will be stretched so that individual fibers begin to break in the failure region.[24] For better understanding of this phenomenon in the stress–strain curve, a loading–unloading test is carried out. As illustrated in Figure 10, the slope of the curve in the unloading cycle is not equal to that in the loading cycle. This observation shows that some fibers experience plastic deformation which causes the nonlinear curve with some unrecoverable deformation. Another important point, which can be realized from this figure, is that, similar to observation in the loading cycle, the slope of the curve in the unloading cycle varies significantly. According to Figure 10, the slope varies at almost the same strain in loading and unloading cycles. The stress–strain curve of collagen fibers is similar to that of the PLA. The same curve was reported for soft tissues as well.[24] Lopatine et al.[25] reported a variation in the slope of the load–displacement response under nano-indentation test of hydroxyapatite thin films.

Figure 11 shows the stress–strain curve obtained in the bulk compression tests. By comparing the presented results in Figures 9 and 11, it is observed that the stress–strain curves in tension and compression do not coincide. This reveals asymmetry in tension and compression.

Since the obtained curves are nonlinear even in small strains, the Hook's law cannot be used to

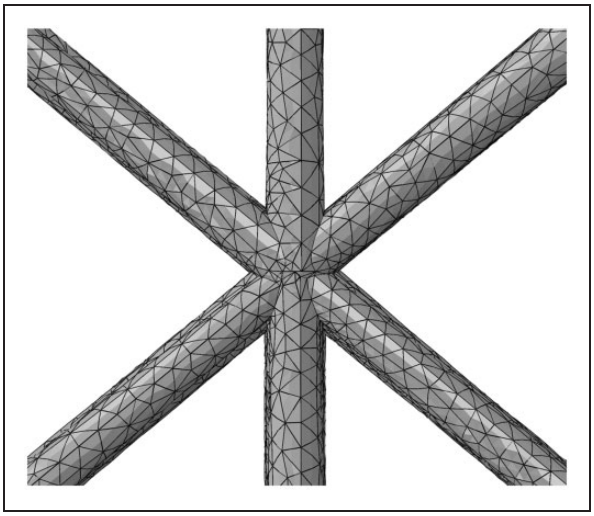

**Figure 8.** The meshed model using C3D10M elements.

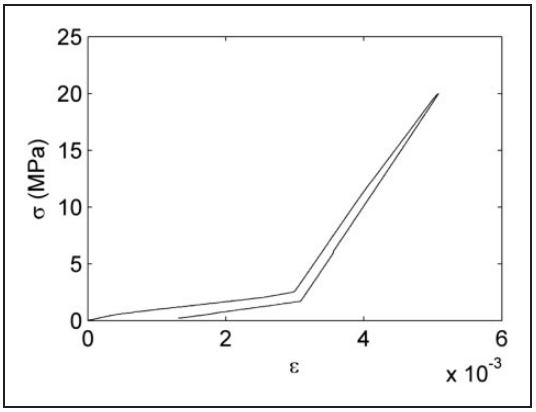


**Figure 10.** Stress–strain curve for loading–unloading tensile test.

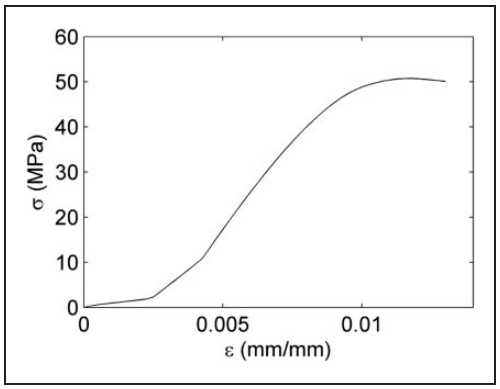


**Figure 9.** The average stress–strain curve for tensile specimens.

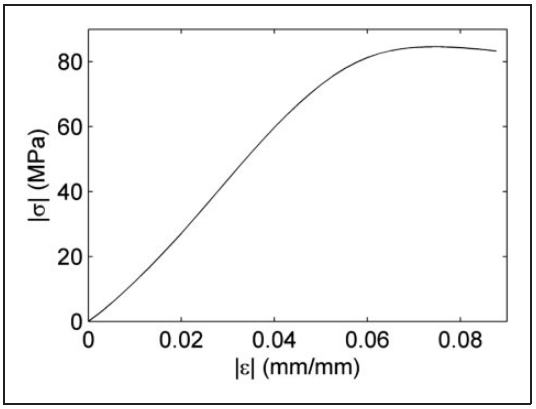


**Figure 11.** The average stress–strain curve for the bulk compression tests.

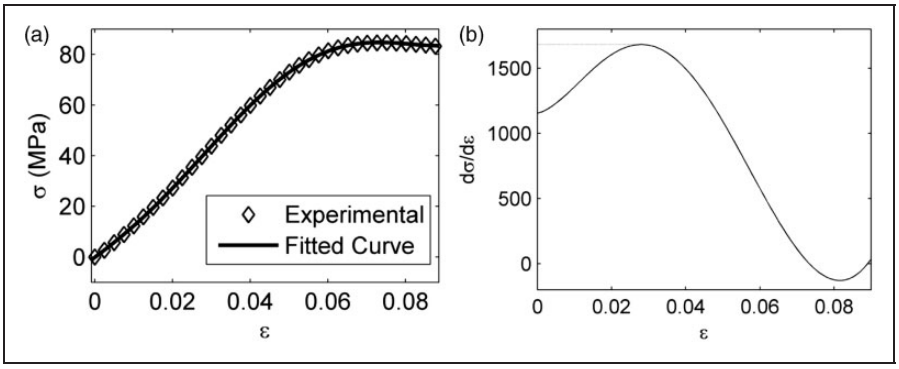


**Figure 12.** (a) The fitted curve to the experimental data. (b) Variations in the derivative of the stress–strain curve to calculate the elastic modulus.

**Table 1.** Elastic moduli of the bulk tension and compression specimens.

| Sample | Tensile | Compressive |
|---|---|---|
| Elastic modulus (MPa) | $8677 \pm 224.43$ | $1684.8 \pm 144.7$ |

calculate the CLS elastic modulus. Therefore, the method presented in ASTM D695, which is suitable for elastomeric foams with highly nonlinear stress–strain curves, is used.[26] In this method, a piecewise polynomial is fitted to the stress–strain curves (Figure 12(a)). Then the polynomial's derivative is plotted as a function of the strain (Figure 12(b)), and its maximum value, corresponding to the maximum slope of the stress–strain curve, is assumed to be the Young's modulus. The calculated elastic moduli in tension and compression are presented in Table 1. This method is used for calculating the elastic modulus of metallic foams.[12]

To calculate the Poisson's ratio ($\nu$), the lateral deformation is measured in several steps and in several points at each step for tension specimens. Then, the average value of each step is used for calculating the Poisson's ratio. Using this method, $\nu = 0$ is obtained. The obtained Poisson's ratio and the stress–strain curve presented in Figure 9 show that the polylactic acid material exhibits brittle behavior.

## Characterization of cellular sandwich structure

The average dimensions of fabricated CLS samples are measured as $37.87 \times 37.78 \times 30.51\,\text{mm}^3$ which reveal deviations from the designed values. Comparison of these numbers with the designed dimensions of the model (that are $36 \times 36 \times 30.21\,\text{mm}^3$ as seen in Figure 3) indicates that the process is more accurate in the fabrication direction than the in-plane ones. It is worth mentioning that the dimensional repeatability of the process is investigated through measuring all dimensions of three produced CLS samples. In addition, the struts' diameter is measured in six points of each strut for each sample and the average value is obtained. This value, which is about 1.482 mm, is then used for the finite element analysis. The CLS's porosity is measured using the Archimedes principle.[3] In this regard, each specimen is tested three times and the average value of the porosity is obtained to be about 90.51%, which is around 99.68% of the porosity obtained from the CAD model.

As discussed in the Mechanical behavior characterization section, the CLS specimens are compressed at the strain rate of $10^{-5}\,\text{S}^{-1}$. The force–displacement response of the structure (not presented here) shows that the load carrying capacity of the structure is about 150 kg. This value is impressing in combination with the weight of the fabricated CLS which is about 5.2 g. Figure 14 shows the average stress–strain curves of the CLSs. The stress is calculated through dividing the applied force by the area parallel to the loading direction, and the strain is calculated by dividing the displacement of the upper platen by the CLS's height. The elastic modulus of the CLS, calculated using the method presented in the previous section, is about $E_{CLS} = 43.07 \pm 0.13\,\text{MPa}$. This number is about 0.50% and 2.55% of that of tensile and compressive specimens, respectively.

## Deformation mechanisms in the structure

The experimental observations show that fabricated parts by additive manufacturing techniques may suffer from structural imperfections. These imperfections can be classified into two categories: micro-(nano-) pores and non-uniform diameter of the struts. These imperfections can affect the deformed configuration of the lattice because of stress concentration around the defects. To be able to distinguish the mechanisms of deformation in the lattice, three CLSs are compressed until their fracture. The deformed lattices show almost the same configuration indicating that the same deformation mechanism is responsible for fracture in all the samples. Figure 15 shows the deformed lattice at a compressive strain of 3.2%. The final configuration is associated with both irregularities in the struts and plastic hinge formed

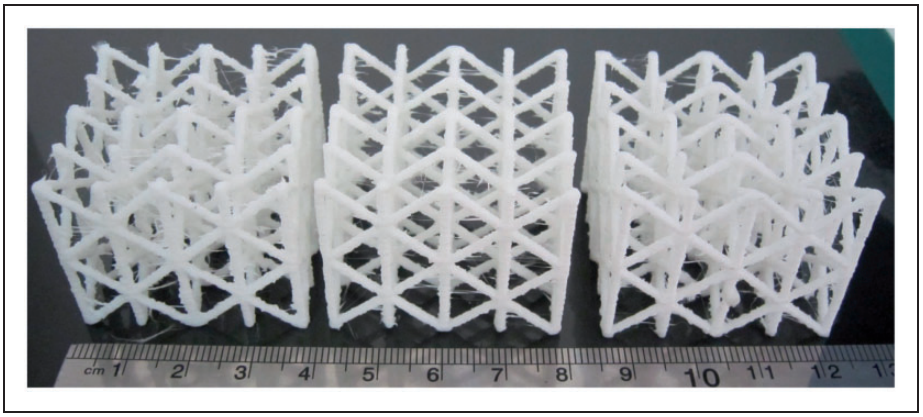

**Figure 13.** Three cellular lattice structures fabricated by the FDM.

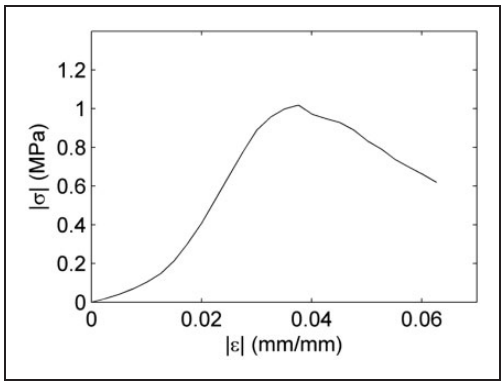


**Figure 14.** The average stress–strain curve of the CLSs.

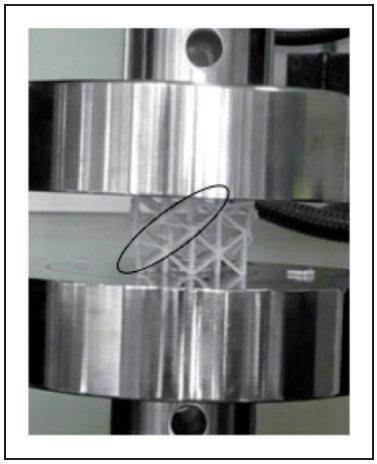

**Figure 15.** Shear band during loading.

near the vertexes after the vertical struts are buckled. Since the diagonal struts in the shear band are broken in the vertices, it is believed that formation of the plastic hinge is more effective than the irregularities. This plastic hinge is formed due to bending in the diagonal struts and leads to the formation of the shear band similar to what has been observed in cellular lattices.[15,27] It is also found that the initial failure occurs locally in the vertical struts due to plastic

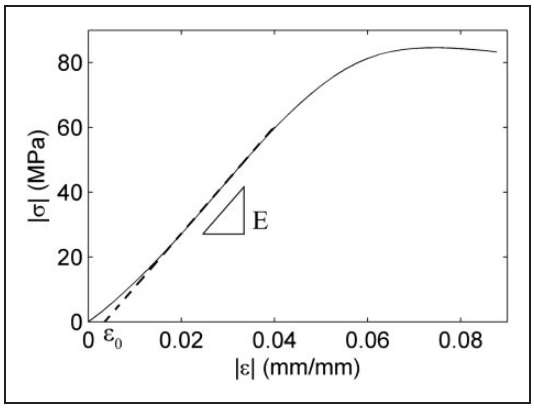


**Figure 16.** The modified stress–strain curve of the uniaxial compression sample for modeling purposes.

deformation and local buckling of the struts. Deformation of the struts located in the edges of the structure is more severe than that of the ones in the middle of the structure. Wen-Yea Jang et al. reported a similar observation in aluminum open-cell foams both experimentally[28] and numerically.[29] They found that deformation is more severe in the lower one-third of the structure. The above-mentioned results are in a good agreement with those reported in the literatures[6,14] for 316 L BCC-Z cellular sandwich microstructures.

## *Finite element modeling*

The geometrical details of the finite element model are presented in the Materials and methods section. In order to specify a suitable bulk material for the struts, the compression stress–strain curve of the bulk material (Figure 11) is attributed to the struts. Since it is not possible to consider the toe region in the model, the stress–strain curve should be modified to a typical one.[30] To do so, the continuation of the linear region of the curve is intersected by the zero-stress axis and the nonlinear region on the left side is removed.[31] This process, which is shown in Figure 16, is performed on the stress–strain responses

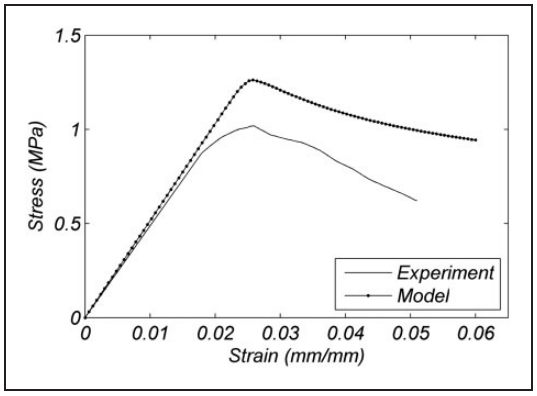


**Figure 17.** Comparison of the modified experimental stress-strain curve of the lattice with the model's prediction.

of the bulk compression sample and the CLS. The latter is done so that the experimental results are comparable with the model's predictions.

A mesh study is first performed to ensure of reasonable accuracy of the finite element results. In this regard, the size of the mesh is reduced until maximum change in the stress–strain curve becomes negligible. Using this method, the appropriate mesh size is obtained to be 0.375.

Figure 17 shows the modified experimental stress–strain curve of the lattice in comparison with the modeling result. The elastic modulus and collapse stress of the lattice are predicted to be about 6% and 23.9% higher than the experimentally measured ones, respectively. As a result, the elastic modulus is well fitted to the experimental one, but the prediction of collapse stress is not well accurate. To understand the reason, it should be noted that deformation of the lattice is small in the elastic region so that only the vertical struts are deformed. Accordingly, the struts just experience the compressive deformation mechanism. By increasing the deformation, the diagonal struts are bent which gives rise to the application of tension to some regions of the struts. Therefore, using just the stress–strain response of compression sample leads to over prediction in the nonlinear region of the response. Notice that the ultimate stress of the compressive sample is about 80 MPa, while this value is about 50 MPa for the tensile one. As another reason, in small deformations, the effects of the struts' imperfections are not vital. However, by increasing the level of the deformation, these effects become more important. The existence of defects causes stress concentration in the defects' site which causes reduction in the amount of the required force to induce deformation.

## Conclusion

In this study, the manufacturability and repeatability of Polylactic Acid BCC-Z CLS fabricated by FDM are investigated. To do so, some CLSs are fabricated and examined in compression. In addition, some bulk tensile and bulk compressive specimens are fabricated to be able to characterize the bulk material of the CLSs' struts. The stress–strain responses of the bulk material in tension and compression illustrate asymmetric material properties. The results show that the stress–strain response of both bulk and CLSs is nonlinear due to un-crimping of the PLA fibers. The elastic modulus of the CLS is $E_{CLS} = 43.07 \pm 0.13$ MPa, which is about 0.50% and 2.55% of bulk tension and compression ones, respectively. Furthermore, to understand the failure of the struts, the deformation mechanisms of CLS are investigated. The observations are shown to be in a good agreement with those reported for 316 L BCC-Z cellular lattice structures. As another consequence of the present study, the load-carrying capacity of the manufactured CLS is found to be about 150 kg, whereas its weight is about 5.2 g. To study the bulk material of the struts, a solid finite element model is developed, too, and the stress–strain response of the compression sample is attributed to the struts. The results show that the elastic response is well predicted by the model. In the plastic region, however, difference between model and experiment is more pronounced because of the effects of microstructural defects, which are not considered in the finite element model. The model predicts the elastic modulus and collapse stress of the lattice to be about 6% and 23.9% higher than the experimentally measured ones, respectively.

### Declaration of Conflicting Interests

The author(s) declared no potential conflicts of interest with respect to the research, authorship, and/or publication of this article.

### Funding

The author(s) received no financial support for the research, authorship, and/or publication of this article.

### References

1. Sun C and Vaidya R. Prediction of composite properties from a representative volume element. *Compos Sci Technol* 1996; 56: 171–179.
2. Cerardi A, et al. Mechanical characterization of polyamide cellular structures fabricated using selective laser sintering technologies. *Mater Des* 2013; 46: 910–915.
3. Yan C, et al. Evaluations of cellular lattice structures manufactured using selective laser melting. *Int J Mach Tools Manuf* 2012; 62: 32–38.
4. Kruth J-P, et al. Part and material properties in selective laser melting of metals. In: *Proceedings of the 16th international symposium on electromachining*, Shanghai, China, 19–23 April 2010.
5. Murat tekin C. *Mechanical characterization and modeling of porous polymeric materials manufactured by selective laser sintring*. MSc thesis, Middle East Technical University, Turkey, December 2009.
6. Gumruk R and Mines R. Compressive behaviour of stainless steel micro-lattice structures. *Int J Mech Sci* 2013; 68: 125–139.

7. Wadley HNG and Queheillalt DT. Thermal applications of cellular lattice structures. *Mater Sci Forum* 2007; 539: 242–247.
8. Babaee S, et al. Mechanical properties of open-cell rhombic dodecahedron cellular structures. *Acta Material* 2012; 60: 2873–2885.
9. Kooistra GW and Wadley HNG. Lattice truss structures from expanded metal sheet. *Mater Des* 2007; 28: 507–514.
10. Kooistra G. Compressive behavior of age hardenable tetrahedral lattice truss structures made from aluminium. *Acta Material* 2004; 52: 4229–4237.
11. Yasa E, et al. Investigation on occurrence of elevated edges in selective laser melting. In: *International solid freeform fabrication symposium*, Austin, TX, 8–10 August 2009.
12. Van Bael S, Vandenbroucke B, Kerckhofs G, et al. Design and production of bone scaffolds with selective laser melting. In: *138th TMS Annual Meeting and Exhibition 2009. Minerals, Metals & Materials Soc*. 15–19 February 2009.
13. Tsopanos S, et al. The influence of processing parameters on the mechanical properties of selectively laser melted stainless steel microlattice structures. *J Manuf Sci Eng* 2010; 132: 041011–1-12.
14. Labeas GN and Sunaric MM. Investigation on the static response and failure process of metallic open lattice cellular structures. *Strain* 2010; 46: 195–204.
15. Santorinaios M, et al. Crush behaviour of open cellular lattice structures manufactured using selective laser melting. *High Performance Struct Mater III* 2006; 85: 481–490.
16. Smith M, Guan Z and Cantwell WJ. Finite element modelling of the compressive response of lattice structures manufactured using the selective laser melting technique. *Int J Mech Sci* 2013; 67: 28–41.
17. Karamooz RMR and Kadkhodaei M. A computationally efficient modeling approach for predicting Mechanical Behavior of Cellular Lattice Structures. *J Mater Eng Performance* 2015; 24(1): 245–252.
18. Wang CC, Lin T-W and Hu S-S. Optimizing the rapid prototyping process by integrating the Taguchi method with the Gray relational analysis. *Rapid Prototyp J* 2007; 13: 304–315.
19. Sood AK, Ohdar RK and Mahapatra SS. Experimental investigation and empirical modelling of FDM process for compressive strength improvement. *J Adv Res* 2012; 3: 81–90.
20. Teitelbaum GA. Proposed build guidelines for use in fused deposition modeleing to reduce build time and material volume. In: *Mechanical engineering*. College Park: University of Maryland, ProQuest, 2009.
21. ASTM, Standard Test Method for Tensile Properties of Plastics, in D 638-03. 2003: United States.
22. ASTM, Standard Test Method for Compressive Properties of Rigid Plastics, in D 695 – 02a. 2002: United States.
23. Karamooz Ravari MR, Kadkhodaei M and Ghaei A. A unit cell model for simulating the stress-strain response of porous shape memory alloys. *J Mater Eng Perform* 2015; 24(10): 4096–4105.
24. Hammer WI. *Functional soft-tissue examination and treatment by manual methods*. Jones & Bartlett Learning, 2007.
25. Lopatin CM, et al. Ion-beam densification of hydroxyapatite thin films. *Nucl Instrument Meth Phys Res B* 1998; 142: 522–531.
26. Kinney JH, et al. Three-dimensional imaging of large compressive deformations in elastomeric foams. *J Appl Polym Sci* 2001; 80: 1746–1755.
27. McKown S, et al. The quasi-static and blast loading response of lattice structures. *Int J Impact Eng* 2008; 35: 795–810.
28. Jang W-Y and Kyriakides S. On the crushing of aluminum open-cell foams Part I. Experiments. *Int J Solids Struct* 2009; 46: 617–634.
29. Jang W-Y and Kyriakides S. On the crushing of aluminum open-cell foams Part II. Analysis. *Int J Solids Struct* 2009; 46: 635–650.
30. Karamooz Ravari MR and Kadkhodaei M. Finite element modeling of the elastic modulus of Ti6Al4V scaffold fabricated by SLM. In: *Poromechanics V: Proceedings of the fifth biot conference on poromechanics*, Vienna, Austria, 10–12 July 2013. ASCE.
31. Karamooz Ravari MR, et al. Numerical investigation on mechanical properties of cellular lattice structures fabricated by fused deposition modeling. *Int J Mech Sci* 2014; 88: 154–161.